

Shadow thermodynamics of AdS black hole with the nonlinear electrodynamics term

He-Bin Zheng(郑何斌), Ping-Hui Mou(牟平辉), Yun-Xian Chen(陈芸仙), and Guo-Ping Li(李国平)

Citation: Chin. Phys. B, 2023, 32 (**8**): 080401. DOI: 10.1088/1674-1056/acc806
Journal homepage: http://cpb.iphy.ac.cn; http://iopscience.iop.org/cpb

What follows is a list of articles you may be interested in

Thermodynamic effects of Bardeen black hole surrounded by perfect fluid dark matter under general uncertainty principle

Zhenxiong Nie(聂振雄), Yun Liu(刘芸), Juhua Chen(陈菊华), and Yongjiu Wang(王永久)
Chin. Phys. B, 2022, 31 (**5**): 050401. DOI: 10.1088/1674-1056/ac3ca8

Thermodynamics and weak cosmic censorship conjecture of charged AdS black hole in the Rastall gravity with pressure

Xin-Yun Hu(胡馨匀), Ke-Jian He(何柯健), Zhong-Hua Li(李中华), Guo-Ping Li(李国平)
Chin. Phys. B, 2020, 29 (**5**): 050401. DOI: 10.1088/1674-1056/ab7daa

A note on the mass of Kerr-AdS black holes in the off-shell generalized ADT formalism

Yi-De Jing(景艺德), Jun-Jin Peng(彭俊金)
Chin. Phys. B, 2017, 26 (**10**): 100401. DOI: 10.1088/1674-1056/26/10/100401

Gravitational quasi-normal modes of static R^2 Anti-de Sitter black holes

Hong Ma(马洪), Jin Li(李瑾)
Chin. Phys. B, 2017, 26 (**6**): 060401. DOI: 10.1088/1674-1056/26/6/060401

Thermodynamics and geometrothermodynamics of regular black hole with nonlinear electrodynamics

Qiao-Shan Gan(甘俏姗), Ju-Hua Chen(陈菊华), Yong-Jiu Wang(王永久)
Chin. Phys. B, 2016, 25 (**12**): 120401. DOI: 10.1088/1674-1056/25/12/120401

Shadow thermodynamics of AdS black hole with the nonlinear electrodynamics term

He-Bin Zheng(郑何斌), Ping-Hui Mou(牟平辉), Yun-Xian Chen(陈芸仙), and Guo-Ping Li(李国平)†

School of Physics and Astronomy, China West Normal University, Nanchong 637000, *China*

(Received 8 February 2023; revised manuscript received 7 March 2023; accepted manuscript online 28 March 2023)

We creatively employ the shadow radius to study the thermodynamics of a charged AdS black hole with a nonlinear electrodynamics (NLED) term. First, the connection between the shadow radius and event horizon is constructed with the aid of the geodesic analysis. It turns out that the black hole shadow radius shows a positive correlation as a function of the event horizon radius. Then in the shadow context, we find that the black hole temperature and heat capacity can be presented by the shadow radius. Further analysis shows that the shadow radius can work similarly to the event horizon in revealing black hole phase transition process. In this sense, we construct the thermal profile of the charged AdS black hole with inclusion of the NLED effect. In the $P < P_c$ case, it is found that the N-type trend of the temperature given by the shadow radius is always consistent with that obtained by using the event horizon. Thus, we can conclude for the charged AdS black hole that the phase transition process can be intuitively presented as the thermal profile in the shadow context. Finally, the effects of NLED are carefully analyzed.

Keywords: AdS black hole, the nonlinear electrodynamics, shadow thermodynamics

PACS: 04.70.Dy, 04.50.Kd, 04.70.–s **DOI:** 10.1088/1674-1056/acc806

1. Introduction

Black holes, predicted by Einstein's general theory of relativity, are very mysterious celestial bodies in the universe. At present, more and more astronomers and physicists devoted themselves to research of black hole physics in theory and experiments. On the theoretical side, one has proved that a black hole is a thermodynamic system, which possesses the temperature, entropy, negative heat capacity, and so on. Also, one has obtained a series of achievements that greatly promoted the development of black hole physics. On the experimental side, the Laser Interferometer Gravitation-Wave Observatory (LIGO) detected the gravitational wave signal produced by the merger of two massive black holes, which provide an effective evidence for black holes.[1] Later, the Event Horizon Telescope (EHT) has reported images of the supermassive black hole M87* and SgrA*, which gave a direct evidence of existence of black holes.[2–7] From those images, it was shown that there always exists a dark central area with a bright ring outside, where the dark region and bright ring are now called the black hole shadow and photon sphere, respectively.

Due to the strong gravitational field, the light rays come from the infinity will be deflected in the neighborhood of black hole. As long as the curvature of the ray approaches to the critical curve, the photons will be asymptotically close to the bound photon orbit. Therefore, when the light rays emitted from a light source behind a black hole, the static observer at infinity can observe that the photons with a radius less than the bound photon orbit will fall into the black hole, which then naturally result in a shadow,[8] while other photons would move to the infinity. This bound orbit gives rise to the so-called photon sphere of black hole. The size and shape of the shadow is determined by the photon sphere. In the case of Schwarzschild black holes, the photon sphere is located at $r = 3M$.[9] Black hole shadows can give us information about the fundamental properties of black holes. Synge and Luminet studied, for the first time, the photon trajectories of Schwarzschild black holes.[10] Later, Bardeen further studied the shadow of the rotating Kerr black hole.[11] Especially in 2017, the results inferred by EHT observations are shown to be consistent with theoretical expectations, thereby further provides an obvious evidence for the existence of black holes in the universe.[12] In recent years, many researchers have been attracted to study the black hole shadows. For instance, one finds that the shadow can be used to test the Lorentz symmetry.[13] By considering accretions surrounding black hole or not, the shadows of different types of black holes and wormholes have also been clearly studied,[14–31] where some important result are obtained.

Moreover, since a black hole can be regarded as a thermodynamic system, many researches have devoted to study its special thermodynamic properties. In fact, the real understanding of the thermal properties of black holes came after the establishment of the four laws of black hole thermodynamics and the discovery of Hawking radiation. Through quantum field theory, Hawking demonstrated that particles can emitted from the event horizon of black hole due to the vacuum fluctuation,[32] which laid a solid foundation for the study of black hole thermodynamics. Under the premise that the cos-

†Corresponding author. E-mail: gpliphys@yeah.net

© 2023 Chinese Physical Society and IOP Publishing Ltd

mic supervision hypothesis and strong energy conditions are true, Hawking proved the Hawking area theorem, that is, the area of a black hole never decreases in a clockwise direction. On this basis, Bekenstein considered the area and surface gravity of the event horizon to be the entropy and temperature of a black hole. Thus, the four laws of black hole thermodynamics gradually formed. At present, there are two main focuses on black hole thermodynamics, one is to establish the basis of the traditional four laws of black hole thermodynamics and the study of thermodynamic quantities, the other is to study black hole thermodynamics in the extended phase space, i.e., regarding the negative cosmological constant as one of the thermodynamic quantities to expand the space of macroscopic states. For instance, Mann *et al.* linked the negative cosmological constant to the pressure in thermodynamic systems, which has attracted many researchers to continue to explore this vision in depth.[33] Later, one found that the thermodynamic system of a charged AdS black hole is very similar to the van der Waals liquid-gas system.[33–38] Meanwhile, Wei studied the dynamic phase behavior of black hole triplic points[39] in the extended phase space, for the first time. More importantly, the relation between the thermodynamic phase structure of black holes and the shadow radius have been preliminary studied in Refs. [40,41]. In a word, both black hole thermodynamics and shadow have always been widely studied in recent years.[33–60]

It should be noted that linking the shadow of black hole with its thermodynamics has an important significance as it can be regarded as a bridge to reflect more information about the black hole thermodynamics. In view of this, the purpose of this paper is to construct the relationship between the shadow radius and the thermodynamic phase transition in the AdS spacetime. We will first study the relationship between the critical thermodynamic phase transition and the black hole shadow. Through a carefully discussion, it is believed that the black hole shadow can indeed be regarded as a powerful tool during revealing the thermodynamic phase transition process of black hole. In Ref. [61], we preliminarily found that the dependence of the black hole shadow and thermodynamics may be structured in the regular spacetime.

On the other hand, the NLED effect in curved spacetime is very important since photons propagate along geodesic lines that are no longer zero in actual Minkowski spacetime, but in corrected effective geometry[62] in this case. Many studies have been devoted to this area in accompany with much fruits.[62–64] In 2000, the geometrical aspects of light propagation in nonlinear electrodynamics have been discussed by Novello *et al.*[62] Novello's method has been apply to derive the effective geometry induced by Euler–Heisenberg NLED effects in regular black hole spacetime.[63] Also, the NLED effects have been taken into account during the study of the optical appearance of black holes.[64] However, it should be noted that the relationship between the shadow radius and thermodynamic for an NLED black hole remains unknown. In view of this, we take the AdS black hole with the NLED term as an example to study thermodynamic phase transition with the shadow radius in this paper.

The rest of this paper are organized as follows. In Section 2, the shadow radius of the AdS black hole with the NLED term is presented, and the critical condition of the black hole phase transition is obtained. In Section 3, the thermodynamic phase transition of black hole is analyzed by using the shadow radius. In Section 4, the thermal profiles of the black holes in several representative sets of coupling constants are established. Section 5 is the conclusions and discussion. Through this study, we use the units $G_{\rm N}=\hbar=\kappa_{\rm B}=c=1$.

2. Shadow radius and critical state

Consider that the action of the NLED theory which minimally coupled to gravity reads[65]

$$S=\frac{1}{16\pi}\int\sqrt{-g}[R+K(\psi)]\mathrm{d}^4x, \tag{1}$$

with

$$\psi=F_{\mu\nu}F^{\mu\nu}, \tag{2}$$

$$F_{\mu\nu}=\nabla_\mu A_\nu-\nabla_\nu A_\mu. \tag{3}$$

Here, R is the Ricci scalar, g is the metric tensor determinant, A_μ is the Maxwell field, $K(\psi)$ is the function of ψ. $\mathcal{L}(\mathcal{F})$ is the NLED Lagrangian depending on electromagnetic invariants, with $\mathcal{F}=\frac{1}{4}F_{\mu\nu}F^{\mu\nu}$ and $F^{\mu\nu}$ denoting the eletromagnetic field strength tensor. The Lagrangian density of the black hole is

$$\mathcal{L}(\mathcal{F})=8\sqrt{2}\zeta\sqrt{-4\mathcal{F}}-16\mathcal{F}-8\Lambda. \tag{4}$$

To study the shadow of black hole, we need to know how photons propagate in this spacetime. Note that the effective geometry induced by the NLED will correct the background geometry along the null geodesics of which photons would usually propagate. In our analysis, we consider that in a nonlinear electrodynamic term, photons propagate along the null geodesics in effective geometry. The propagation path of photons can be described by null geodesics in effective spacetime, that is,[62,63,66,67]

$$g^{\mu\nu}_{\rm eff}=\mathcal{L}_{\mathcal{F}}g^{\mu\nu}-\mathcal{L}_{\mathcal{F}\mathcal{F}}F^{\mu}_{\alpha}F^{\alpha\nu}, \tag{5}$$

where $\mathcal{L}_{\mathcal{F}}\equiv\partial\mathcal{L}/\partial\mathcal{F}$. The effective geometry of the metric can be rewritten as

$$\mathrm{d}s^2_{\rm eff}=H(r)\left[-f(r)\mathrm{d}t^2+\frac{\mathrm{d}r^2}{f(r)}\right]+h(r)r^2\mathrm{d}\Omega^2, \tag{6}$$

in which $H(r)=-\mathcal{L}_{\mathcal{F}}$ and $h(r)=-\mathcal{L}_{\mathcal{F}\mathcal{F}}\frac{Q^2}{r^4}$ for metric (23). Therefore, we have

$$H(r)=1+\frac{r^2\zeta}{Q},\quad h(r)=1+\frac{2r^2\zeta}{Q}. \tag{7}$$

Note that the functions $H(r)$ and $h(r)$ must be positive, because we want the photon that does not change its own characteristics during motion.[64] Based on Eq. (6), the Lagrangian of density, $\mathcal{L}$, reads

$$\mathcal{L}=\frac{1}{2}\left[H(r)(f(r)\dot{t}^2-f(r)^{-1}\dot{r}^2)-h(r)r^2(\dot{\theta}^2+\sin^2\theta\dot{\phi}^2)\right], \tag{8}$$

where $\dot{x}\equiv \mathrm{d}x/\mathrm{d}\tau$, the τ is the affine parameter. Since we only consider the photons that move on the equatorial plane ($\theta=\pi/2$, $\dot{\theta}=0$ and $\ddot{\theta}=0$), the metric function does not contain time t and azimuthal angle ϕ. Thus, the associated equation of conserved constants can be obtained as follows:

$$p_t=\frac{\partial\mathcal{L}}{\partial\dot{t}}=H(r)f(r)\dot{t}=E, \tag{9}$$

$$p_\phi=\frac{\partial\mathcal{L}}{\partial\dot{\phi}}=h(r)r^2\dot{\phi}\sin^2\theta=L, \tag{10}$$

where E and L represent the energy and angular momentum of photon. The derivatives of time, radial, and azimuthal angle components can be obtained as follows:

$$\frac{\mathrm{d}t}{\mathrm{d}\tau}=\frac{1}{bH(r)f(r)}, \tag{11}$$

$$\frac{\mathrm{d}r}{\mathrm{d}\tau}=\sqrt{\frac{1}{b^2H(r)^2}-\frac{f(r)}{r^2H(r)h(r)}}, \tag{12}$$

$$\frac{\mathrm{d}\phi}{\mathrm{d}\tau}=\pm\frac{1}{r^2h(r)}, \tag{13}$$

in which the symbol $\pm$ indicates the clockwise $(+)$ and counterclockwise $(-)$ direction of the motion of photon. Here, b is the impact parameter, satisfying $b=|L|/E$. The equations of motion for the null geodesic is

$$H(r)f(r)\dot{t}^2-H(r)f(r)^{-1}\left(\frac{\mathrm{d}r}{\mathrm{d}\phi}\right)^2\dot{\phi}^2-r^2h(r)\dot{\phi}^2=0. \tag{14}$$

The above three formulas report a complete description of the photon dynamics around the black hole, where the effective potential can be written as

$$\left(\frac{\mathrm{d}r}{\mathrm{d}\tau}\right)^2+\mathcal{V}_{\mathrm{eff}}(r)=0, \tag{15}$$

with the effective potential

$$\mathcal{V}_{\mathrm{eff}}(r)=\frac{1}{r^2H(r)h(r)}f(r)-\frac{E^2}{L^2H(r)^2}. \tag{16}$$

It is obvious that $V_{\mathrm{eff}}(r)$ determines the position of an unstable orbit. This position should satisfy the conditions

$$\mathcal{V}_{\mathrm{eff}}(r)=0,\quad \mathcal{V}'_{\mathrm{eff}}(r)=0,\quad \mathcal{V}''_{\mathrm{eff}}(r)>0. \tag{17}$$

After substituting Eq. (16) into Eq. (17), we have $\frac{L}{E}=\frac{r_{\mathrm{p}}}{\sqrt{f(r_{\mathrm{p}})}}$, where r_{p} is the radius of the photon ring. Substituting Eq. (12) into Eq. (13) yields

$$\frac{\mathrm{d}r}{\mathrm{d}\phi}=\left(\frac{\mathrm{d}r}{\mathrm{d}\tau}\right)/\left(\frac{\mathrm{d}\phi}{\mathrm{d}\tau}\right)=\pm r\sqrt{\frac{r^2E^2h(r)^2}{L^2H(r)^2}-\frac{h(r)}{H(r)}f(r)}. \tag{18}$$

The turning point of the photon orbit is interpreted mathematically by the constraint $\frac{\mathrm{d}r}{\mathrm{d}\phi}|_{r=\chi}=0$, so Eq. (18) can be rewritten as

$$\frac{\mathrm{d}r}{\mathrm{d}\phi}=\pm r\sqrt{\frac{r^2f(\chi)h(r)^2}{\chi^2H(r)^2}-\frac{h(r)}{H(r)}f(r)}. \tag{19}$$

A light ray sends from a static observer placed at r_{O} and transmits into the past with an angle β,[41,68,69]

$$\cot\beta=\left.\frac{\sqrt{g_{rr}}}{\sqrt{g_{\phi\phi}}}\right|_{r=r_{\mathrm{O}}}=\pm\sqrt{\frac{r_{\mathrm{O}}^2h(r_{\mathrm{O}})f(\chi)}{\chi^2H(r_{\mathrm{O}})f(r_{\mathrm{O}})}-1}. \tag{20}$$

With the aid of Eq. (19), we have

$$\sin^2\beta=\frac{\chi^2H(r_{\mathrm{O}})f(r_{\mathrm{O}})}{r_{\mathrm{O}}^2h(r_{\mathrm{O}})f(\chi)}. \tag{21}$$

At the position r_{O}, the shadow radius of the black hole observed by a static observer is given by

$$r_{\mathrm{ss}}=r_{\mathrm{O}}\sin\beta=\chi\sqrt{\frac{H(r_{\mathrm{O}})f(r_{\mathrm{O}})}{h(r_{\mathrm{O}})f(\chi)}}|_{\chi\to r_{\mathrm{p}}}. \tag{22}$$

Next, we further discuss the relationship between the shadow radius and the horizon radius in a exact black hole solution. Recently, Yu and Gao have obtained the exact black hole solution to Einstein gravity with nonlinear electrodynamic field, which is very different from the RN-AdS solution in Einstein–Maxwell gravity with a cosmological constant. The metric can be written as[65]

$$f(r)=1-\frac{2M}{r}+\frac{Q^2}{r^2}-\frac{\Lambda r^2}{3}-\frac{r^2\zeta^2}{3}+2Q\zeta, \tag{23}$$

where ζ, Λ, M, and Q are the coupling constant, cosmological constant, the mass, and charge of black hole, respectively. The horizon radius is the largest root of $f(r_{\mathrm{h}})=0$. In this case, the black hole mass can be written as a function of r_{h},

$$M=\frac{3Q^2+3r_{\mathrm{h}}^2+8P\pi r_{\mathrm{h}}^4+6Qr_{\mathrm{h}}^4\zeta-r_{\mathrm{h}}^4\zeta^2}{6r_{\mathrm{h}}}. \tag{24}$$

The Hawking temperature is

$$T=\frac{f'(r)}{4\pi}|_{r=r_{\mathrm{h}}}=\frac{-Q^2+r_{\mathrm{h}}^2+2Qr_{\mathrm{h}}^2\zeta+r_{\mathrm{h}}^4(8P\pi-\zeta^2)}{4\pi r_{\mathrm{h}}^3}. \tag{25}$$

The state equation can be written as

$$P=\frac{Q^2}{8\pi r_{\mathrm{h}}^4}-\frac{1}{8\pi r_{\mathrm{h}}^2}+\frac{T}{2r_{\mathrm{h}}}-\frac{Q\zeta}{4\pi r_{\mathrm{h}}^2}+\frac{\zeta^2}{8\pi}. \tag{26}$$

According to the definition of entropy,

$$S=\frac{A}{4}=\pi r_{\mathrm{h}}^2, \tag{27}$$

where A is the surface area of the black hole. Equation (24) can be rewritten in terms of pressure and entropy as

$$M(S,Q,P)=\frac{3\pi^2Q^2+3\pi S+8P\pi S^2+6\pi QS\zeta-S^2\zeta^2}{6\pi^{3/2}\sqrt{S}}. \tag{28}$$

The electric potential Φ is

$$\Phi=\frac{\pi Q+S\zeta}{\sqrt{\pi}\sqrt{S}}. \tag{29}$$

Differential for Eq. (28) is

$$\mathrm{d}M=\frac{4S^{3/2}}{3\sqrt{\pi}}\mathrm{d}P+\Big(\frac{\sqrt{\pi}Q}{\sqrt{S}}+\frac{\sqrt{S}\zeta}{\sqrt{\pi}}\Big)\mathrm{d}Q+\Big(-\frac{\sqrt{\pi}Q^2}{4S^{3/2}}+\frac{1}{4\sqrt{\pi}\sqrt{S}}+\frac{2P\sqrt{S}}{\sqrt{\pi}}+\frac{Q\zeta}{2\sqrt{\pi}\sqrt{S}}-\frac{\sqrt{S}\zeta^2}{4\pi^{3/2}}\Big)\mathrm{d}S, \tag{30}$$

combining Eqs. (25)–(27) and (29), it can be easily verified that Eq. (31) satisfies the first law of thermodynamics, i.e.,

$$\mathrm{d}M=T\mathrm{d}S+\Phi\mathrm{d}Q+V\mathrm{d}P. \tag{31}$$

Using the metric function and the effective potential, one can obtain the photon circular orbit radius in this spacetime, i.e.,

$$r_{\mathrm{p}}=\frac{432\pi P-54\zeta^2}{3\times2^{\frac{2}{3}}(8\pi P-\zeta^2)W}-\frac{W}{6\times2^{\frac{1}{3}}(8\pi P-\zeta^2)}, \tag{32}$$

$$W\equiv\sqrt[3]{-2268\zeta^4M+Z-145152\pi^2MP^2+36288\pi\zeta^2MP}, \tag{33}$$

$$Z\equiv\sqrt{(-2268\zeta^4M-145152\pi^2MP^2+36288\pi\zeta^2MP)^2+4(432\pi P-54\zeta^2)^3}. \tag{34}$$

Combining Eq. (22), the shadow radius of the RN-AdS black hole with the effects of NLED can be written as

$$r_{\mathrm{s}}=r_{\mathrm{p}}\sqrt{\frac{H(r_{\mathrm{O}})f(r_{\mathrm{O}})}{h(r_{\mathrm{O}})f(r_{\mathrm{p}})}}. \tag{35}$$

Combining Eqs. (23), (32) and (35), we can obtain the specific expression of the shadow radius as follows:

$$r_{\mathrm{s}}=\frac{\sqrt{3}CC\times\sqrt{\frac{f(r_{\mathrm{O}})}{AA+BB}}}{2\sqrt[3]{DD}(\zeta^2-3)}, \tag{36}$$

where

$$\begin{aligned}
AA\equiv&\ \frac{2\pi CC^2P}{\sqrt[3]{DD^2(\zeta^2-3)^2}}-\frac{CC^2\zeta^2}{4\sqrt[3]{DD^2}(\zeta^2-3)^2}\\
&+\frac{12\sqrt[3]{DD^2}(\zeta^2-3)^2Q^2}{CC^2},\\
BB\equiv&\ \frac{2\sqrt[3]{DD}(\zeta^2-3)(r_{\mathrm{h}}^4(\zeta^2-8\pi P)-3Q^2-6\zeta Qr_{\mathrm{h}}^2-3r_{\mathrm{h}}^2)}{CCr_{\mathrm{h}}}\\
&+6\zeta Q+3,\\
CC\equiv&\ -18+6\zeta^2+\sqrt[3]{DD^2},\\
DD\equiv&\ \frac{1}{r_{\mathrm{h}}}\Big\{189(-Q^2-r_{\mathrm{h}}^2-r_{\mathrm{h}}^4)-378Qr_{\mathrm{h}}^2\zeta+126Q^2\zeta^2\\
&+126r_{\mathrm{h}}^2\zeta^2+189r_{\mathrm{h}}^4\zeta^2+252Qr_{\mathrm{h}}^2\zeta^3\\
&-21Q^2\zeta^4-21r_{\mathrm{h}}^2\zeta^4-63r_{\mathrm{h}}^4\zeta^4-42Qr_{\mathrm{h}}^2\zeta^5+7r_{\mathrm{h}}^4\zeta^6\\
&+\frac{r_{\mathrm{h}}}{27}\Big\{\frac{1}{r_{\mathrm{h}}^2}\Big[r_{\mathrm{h}}^2(162-54\zeta^2)^3+35721(-3+\zeta^2)^4\\
&\times[3Q^2+3r_{\mathrm{h}}^2+6Qr_{\mathrm{h}}^2\zeta-r_{\mathrm{h}}^4(-3+\zeta^2)]^2\Big]\Big\}^{1/2}\Big\}.
\end{aligned}$$

Using the state Eq. (26) and the critical condition

$$(\partial P/\partial r_{\mathrm{h}})=(\partial^2P/\partial r_{\mathrm{h}}^2)=0, \tag{37}$$

one can reach

$$P_{\mathrm{c}}=\frac{1+4Q\zeta+16Q^2\zeta^2}{96\pi Q^2}, \tag{38}$$

$$r_{\mathrm{c}}=\frac{\sqrt{6}Q}{\sqrt{1+2\zeta}}, \tag{39}$$

$$T_{\mathrm{c}}=\frac{(1+2Q\zeta)^{3/2}}{3\sqrt{6}\pi Q}. \tag{40}$$

Due to the fact that the static observer always locates at spatial infinity, we have the constraint $f(r_{\mathrm{O}})=1$ for $r_{\mathrm{O}}=100$.[40] Therefore, we have fixed the location of the observer at $r_{\mathrm{O}}=100$ in Fig. 1. The three graphs in Fig. 1 describe the shadow radius of black hole as a function of the event horizon radius for different values of the coupling constant ζ. It can be seen that when the event horizon radius r_{h} increases, the shadow radius r_{s} will increase. The trend of r_{s} will become gradually flatter with increase of r_{h}. This means that there exists a positive correlation between r_{h} and r_{s}, so that one can employ the shadow radius to present the Hawking temperature of black hole. In addition, the coupling constant decreases the event horizon radius, and meanwhile decreases the shadow radius. When the coupling constant $\zeta\to0$, this black hole will reduce to the RN-AdS black hole. As $\zeta\to0$, the expression (36) can be used to describe the relationship between the shadow radius and the event horizon radius of the RN-AdS black hole. For the RN-AdS black hole, it also exhibits the positive correlation between r_{h} and r_{s}. Therefrom, it is believed that the shadow radius can work similarly to the event horizon radius for describing the black hole temperature.

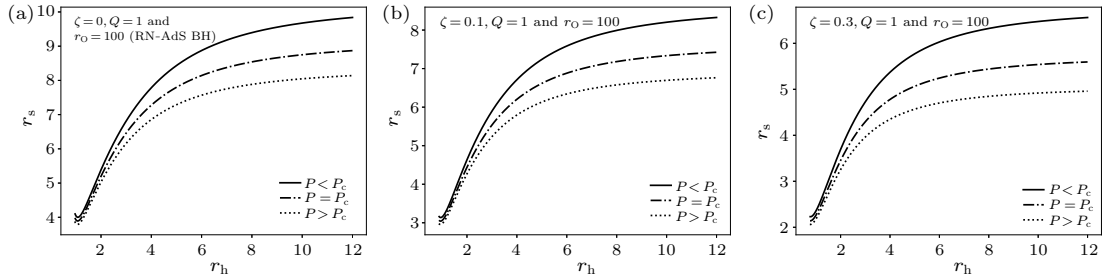


Fig. 1. The variation of shadow radius r_s in terms of the event horizon radius r_h for the charged AdS black hole with nonlinear electrodynamic field: (a) coupling constant $\zeta = 0$ and $r_O = 100$ (RN-AdS black hole), (b) coupling constant $\zeta = 0.1$ and $r_O = 100$, (c) coupling constant $\zeta = 0.3$ and $r_O = 100$. The solid lines, segment dotted lines and dotted lines correspond to $P < P_c$, $P = P_c$ and $P > P_c$, respectively.

3. Phase transition of a charged AdS black hole with nonlinear electrodynamics term by using shadow analysis

In this section, we further discuss the thermodynamic phase transition of the charged AdS black hole with the nonlinear electrodynamics term. According to the Hawking temperature Eq. (26), one can easily see that the black hole temperature works as a function of the radius of the event horizon. As long as the coupling constant is fixed to some certain value, the temperature of the black hole will vary with the radius of the event horizon, as shown in Fig. 2(a). Black hole temperature, as a continuous function of its event horizon radius, exhibits different properties for different values of pressure. In Fig. 2, it can be seen that when $(P > P_c)$, the function image is a monotonically increasing smooth curve, and its slope first decreases and then increases, but would never decrease to zero. In this case, the curve has no inflection point and black hole is in the supercritical phase. When $(P = P_c)$, the function still monotonically increases. However, its slope first decreases to zero, and then begins to increase. This curve corresponds to the critical isobaric, which has an inflection point. In this case, black hole is thermodynamically unstable. When $(P < P_c)$, the function is no longer a monotonous curve, but first increases, then decreases and finally increases. When the pressure is lower than the critical pressure, there are two-phase transition branches. One is in the small radius region, which corresponds to the fluid phase of the van der Waals system, the other is in the large radius region, which corresponds to the gas phase.

In Figs. 2(b) and 2(c), we present curves of black hole temperature as a function of shadow radius for different values of pressure. Figures 2(b) and 2(c) correspond to the coupling constants of $\zeta = 0.1$ and $\zeta = 0.3$, respectively. By choosing some representative values of the coupling coefficient ζ, it is true that one can employ the shadow radius instead of the event horizon to study the process of black hole phase transition. When the pressure is less than the critical pressure, the case of $r_s < r_{s1}$ corresponds to a stable small black hole; and $r_s > r_{s2}$ corresponds to a large stable black hole; while the case of $r_{s1} < r_s < r_{s2}$ corresponds to the unstable state of black hole. Also, we find that a larger value of ζ gives rise to a stronger phase transition temperature, but a smaller value of shadow radius. Meanwhile, Maxwell's equal area theorem can be constructed in T–r_h plane, $T_{h0}(r_{h2} - r_{h1}) = \int_{r_{h2}}^{r_{h1}} T\,\mathrm{d}r_h$. However, when we construct it in T–r_s plane, $T_{s0}(r_{s2} - r_{s1}) \neq \int_{r_{s2}}^{r_{s1}} T\,\mathrm{d}r_s$, the left side of the inequality is slightly smaller than the right side. It may be the following reason why they are not equal. As can be seen from Fig 1, the shadow radius and the radius of the event horizon are not proportional to each other, but only positively correlated.

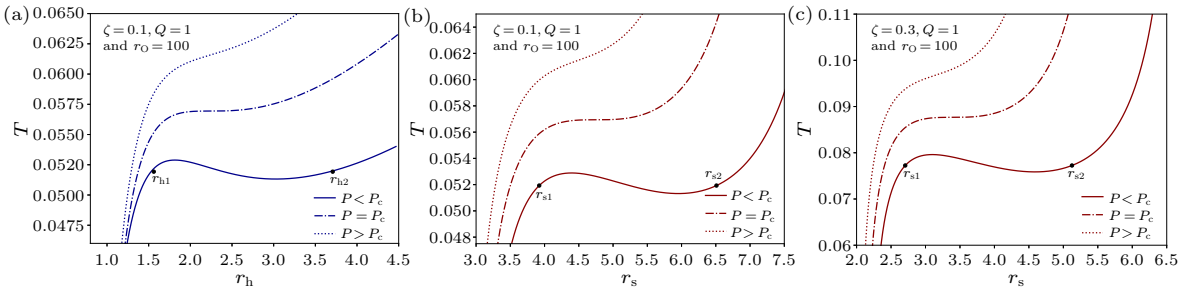


Fig. 2. (a) Temperature as a function of r_h with $\zeta = 0.1$, (b) temperature as a function of r_s with $\zeta = 0.1$, (c) temperature as a function of r_s with $\zeta = 0.3$. A static observer is located at $r_O = 100$.

In addition, the phase transition grade is closely related to the heat capacity of black hole. Specifically speaking, the second-order phase transition at the thermodynamic critical point of the black hole can be represented by the heat capacity mutation and specific heat diverge. By considering the relationship $(S = A/4 = \pi r_h^2)$ and the temperature Eq. (26), we can

obtain the heat capacity of black hole under constant pressure, i.e.,

$$C_P = T\left(\frac{\mathrm{d}S}{\mathrm{d}T}\right)_{P,\zeta} = \frac{2\pi r_{\mathrm{h}}^2[Q^2 - r_{\mathrm{h}}^2 - 2Qr_{\mathrm{h}}^2\zeta + r_{\mathrm{h}}^4(-8P\pi + \zeta^2)]}{-3Q^2 + r_{\mathrm{h}}^2 + 2Qr_{\mathrm{h}}^2\zeta + r_{\mathrm{h}}^4(-8P\pi + \zeta^2)}. \tag{41}$$

Figure 3(a) shows the heat capacity as a function of the radius of the event horizon at different critical pressures. The heat capacities as a function of shadow radius for different critical pressures are shown in Figs. 3(b) and 3(c). It can be seen that the heat capacity diverges at the critical point, which implies the emergence of the second-order phase transition of black hole. In Figs. 3(b) and 3(c), the similar phenomenon of heat capacity also appears at the critical point, thereby the shadow radius can be used to reveal the black hole phase transition.

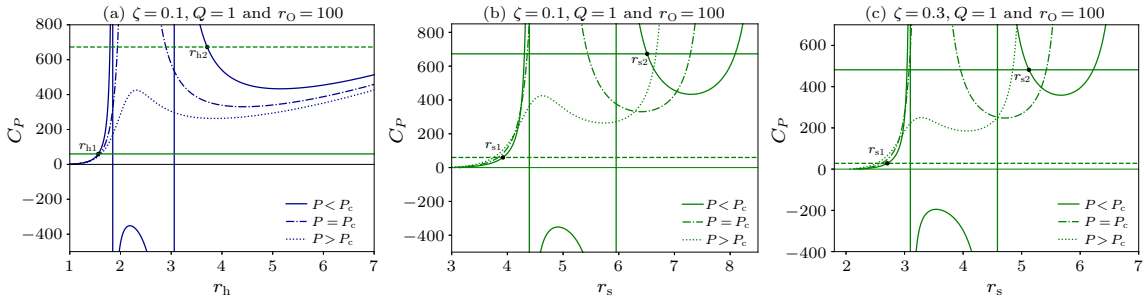


Fig. 3. (a) Heat capacity as a function of r_{h} with $\zeta = 0.1$, (b) heat capacity as a function of r_{s} with $\zeta = 0.1$, (c) heat capacity as a function of r_{s} with $\zeta = 0.3$. A static observer is located at $r_{\mathrm{O}} = 100$.

4. Thermal profile of a charged AdS black hole with nonlinear electrodynamics term

In this section, we use the thermal profile of black hole to intuitively show the relationship between the shadow and the phase structure of black hole. The shadow contour curves of celestial coordinates can be expressed as[70]

$$x = \lim_{r\to\infty}\left(-r^2 \sin\theta_0 \frac{\mathrm{d}\Phi}{\mathrm{d}r}\right)_{\theta_0\to\frac{\pi}{2}}, \tag{42}$$

$$y = \lim_{r\to\infty}\left(r^2 \frac{\mathrm{d}\theta}{\mathrm{d}r}\right)_{\theta_0\to\frac{\pi}{2}}. \tag{43}$$

For a static observer, the shadow contour is shown in Fig. 4. The radius of the shadow contour is greatly affected by the pressure. It is easy to see that the shadow radius decreases with the increasing pressure. The green dotted line represents $P > P_{\mathrm{c}}$, the black hole in this case is at the supercritical phase. The orange segment dotted line is $P = P_{\mathrm{c}}$, the black hole is just at critical pressure, and the shadow in this case is more obvious compared to the supercritical case. The blue dotted line corresponds to $P < P_{\mathrm{c}}$, which shows the shadow profile is in the large radius region. It is worth mentioning that as the coupling constant increases, the shadow radius decreases, which can be easily observed in Fig. 4.

Combining Fig. 2 with Fig. 4, we can build black hole thermal profiles with the aid of the temperature-shadow radius function. Under several representative values of coupling constant ζ, Fig. 5 present three different scenarios: $P > P_{\mathrm{c}}$, $P = P_{\mathrm{c}}$, $P < P_{\mathrm{c}}$. We provide the results in Figs. 5(a)–5(f) in sequence. Figures 5(a) and 5(d) present the thermal distribution of a black hole under supercritical phase $P > P_{\mathrm{c}}$. They have a smaller shadow radius. The temperature of black hole gradually increases from the center of the shadow to the boundary. This case corresponds to the dotted lines in Fig. 2. Figures 5(b) and 5(e) present unstable black holes in a critical state $P = P_{\mathrm{c}}$. In this critical region, the black hole is thermodynamically unstable. The shadow radius of black hole is larger than that of the black hole in the supercritical state. This case corresponds to the segment dotted lines in Fig. 2. Figures 5(c) and 5(f) show the black hole with the pressure that is less than the critical value $P < P_{\mathrm{c}}$. The temperature of black hole in this state has a dramatic trend from inside to outside. The temperature of a black hole increases, then decreases, and finally increases again. We name this change is an "N-type" change. Therefore, it can be seen that the N-type change of temperature with r_{s} in the celestial coordinate is always full consistent with the previous analysis results, i.e., Fig. 2.

To see the N-type change more clearly, we focus on the range of r_{s} in $r_{\mathrm{s1}} \to r_{\mathrm{s2}}$. The results obtained are presented in Fig. 6. Finally, it turns out that the effects of the coupling constant on the phase transition of a charged AdS black hole can also be clearly seen in the shadow context from Fig. 6, which is in agreement with that obtained in Fig. 2.

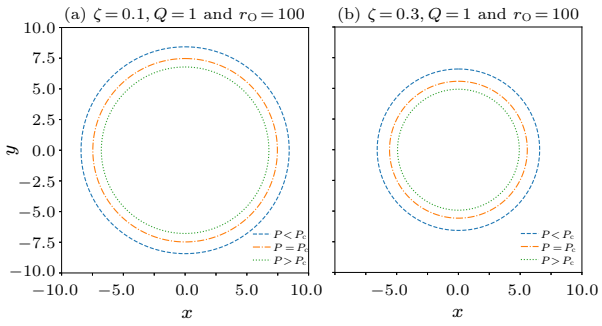


Fig. 4. Shadow cast of the RN-AdS black hole with the effects of NLED: (a) coupling constant $\zeta = 0.1$, (b) coupling constant $\zeta = 0.3$, for the black-hole mass $M = 60$ and $r_{\mathrm{O}} = 100$.

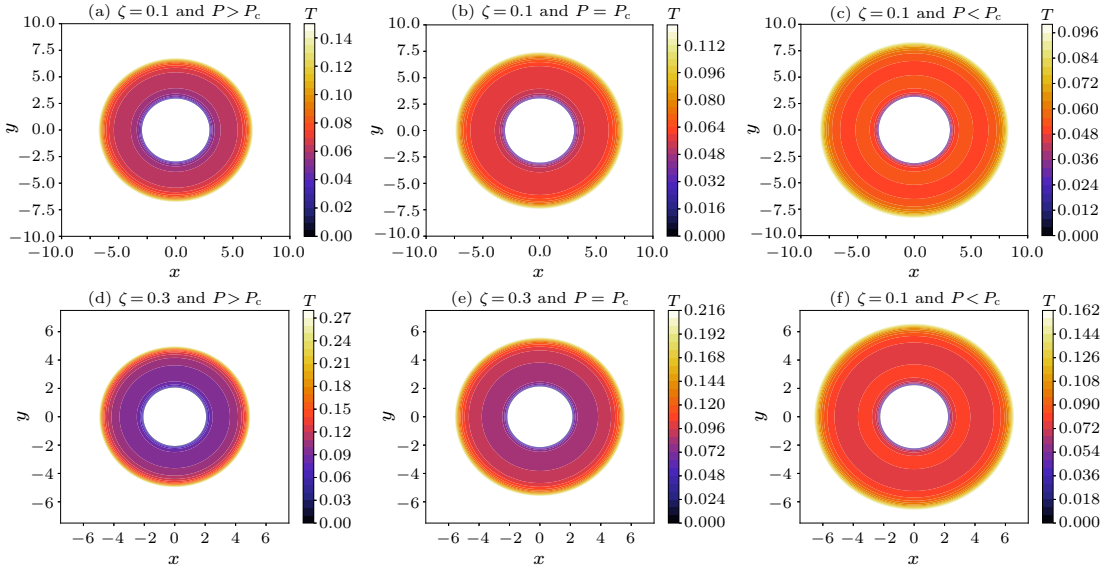


Fig. 5. Thermal profile of the Reissner–Nordström-AdS black hole with the effects of NLED for different thermodynamical cases. (a) $P > P_c$ with $\zeta = 0.1$, (b) $P = P_c$ with $\zeta = 0.1$, (c) $P < P_c$ with $\zeta = 0.1$, (d) $P > P_c$ with $\zeta = 0.3$, (e) $P = P_c$ with $\zeta = 0.3$, (f) $P < P_c$ with $\zeta = 0.3$. The black-hole mass is taken as $M = 60$.

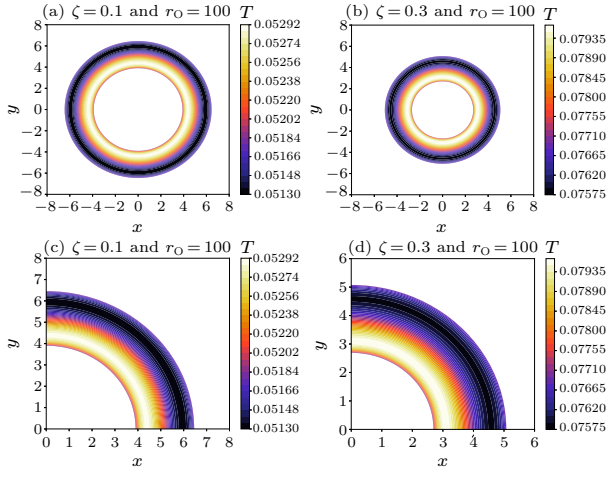


Fig. 6. Thermal profile of a charge AdS black hole with NLED term for different thermodynamical cases: (a) $P < P_c$ with $\zeta = 0.1$, (b) $P < P_c$ with $\zeta = 0.3$, (c) $P < P_c$ with $\zeta = 0.1$, (d) $P < P_c$ with $\zeta = 0.3$. Here (c) and (d) are quarters of (a) and (b), respectively. The black hole mass is taken as $M = 60$.

5. Discussion and conclusion

In summary, we have used the shadow radius instead of the horizon radius to analyze the phase transition of a charged AdS black hole with the NLED term. First, the relationship between the shadow radius r_s and event horizon radius r_h is established with the aid of the corrected effective geometry which is caused by the NLED term. The results shows that they have a positive correlation, implying that black hole temperature can also be established with the shadow radius. When the coupling constant $\zeta \to 0$, the expression (36) can also be used to describe the relationship between the shadow radius and the event horizon in the RN-AdS black hole. In Fig. 1, we present this relationship, and find that if the event horizon radius r_h increases, the shadow radius r_s will increase. The trend of r_s will become gradually flatter with increase of r_h. In view of this, we believe that the shadow can be used to present the phase transition structure of black hole thermodynamics.

Then, we further construct the T–r_s function on the basis of the T–r_h function, and carefully analyze the phase transition curve of the AdS black hole. In the supercritical state ($P > P_c$), the T–r_s curve has no inflection point. In a critical state ($P = P_c$), black holes are in an unstable state. Below the critical pressure ($P < P_c$), there exhibits a two-phase transition branch of black hole. When the shadow radius is small ($r_s < r_{s1}$), it corresponds to a stable small black hole. The case ($r_s > r_{s2}$) corresponds to a stable large black hole, while the unstable intermediate branch appears in the range ($r_{s1} < r_s < r_{s2}$). All of those features well coincide with those obtained by using r_h. Then, combining the relationship between the heat capacity and the event horizon radius, the relationship between the heat capacity and the shadow radius is established to address phase transition grade, as shown in Fig. 3. One can see that the heat capacity diverges at the critical point, which implies the emergence of the second-order phase transition of black hole, which is also consistent with that given by r_h. Finally, based on the function T–r_s, the thermal profiles of the black holes in several representative sets of coupling constants are established. We find that the shadow radius is closely related to the pressure. As the pressure increases, the shadow radius will decrease, but the black hole temperature will increase. When $P < P_c$, the temperature variation law of the black hole exhibits in sequence of increasing → decreasing → increasing, named as N-type. That is to say, the thermodynamics of black holes can be completely reflected on the thermal profile, and the black hole shadow can also reflect the thermodynamic phase transition relationship of black holes in a charged AdS black hole with the NLED term.

In addition, the effects of the coupling coefficient ζ on thermodynamic phase transition have also been discussed. Combined with the above-mentioned facts, we can conclude that the shadow can indeed replace the event horizon, which opens a new door for the study of thermodynamic phase transition of black hole. Finally, the effects of NLED have been carefully analysed through out the paper.

Acknowledgements

This work was supported by the National Natural Science Foundation of China (Grant No. 11903025), the Starting Fund of China West Normal University (Grant No. 18Q062), the Sichuan Youth Science and Technology Innovation Research Team (Grant No. 21CXTD0038), the Chongqing Science and Technology Bureau (Grant No. csts2022ycjh-bgzxm0161), and the Natural Science Foundation of Sichuan Province (Grant No. 2022NSFSC1833).

References

[1] Abbott B P *et al.* (LIGO Scientific, Virgo) 2016 *Phys. Rev. Lett.* **116** 061102
[2] Akiyama K *et al.* (Event Horizon Telescope) 2019 *Astrophys. J. Lett.* **875** L1
[3] Akiyama K *et al.* (Event Horizon Telescope) 2019 *Astrophys. J. Lett.***875** L2
[4] Akiyama K *et al.* (Event Horizon Telescope) 2019 *Astrophys. J. Lett.* **875** L3
[5] Akiyama K *et al.* (Event Horizon Telescope) 2019 *Astrophys. J. Lett.* **875** L4
[6] Akiyama K *et al.* (Event Horizon Telescope) 2019 *Astrophys. J. Lett.* **875** L5
[7] Akiyama K *et al.* (Event Horizon Telescope) 2019 *Astrophys. J. Lett.* **875** L6
[8] Bozza V 2010 *Gen. Rel. Grav.* **42** 2269
[9] Perlick V and Tsupko O Y 2022 *Phys. Rep.* **947** 1
[10] Synge J L 1966 *Mon. Not. R. Astron. Soc.* **131** 463
[11] Bardeen J M, Press W H and Teukolsky S A 1972 *Astrophys. J.* **178** 347
[12] Broderick A E, Pesce D W, Gold R, *et al.* 2022 *Astrophys. J.* **935** 61
[13] Wang H M and Wei S W 2022 *Eur. Phys. J. Plus* **137** 571
[14] Shao W W, Cheng P, Zhong Y and Zhou X N 2015 *J. Cosmol. Astropart. Phys.* **08** 004
[15] Shao W W, Zou Y C, Liu Y X and Mann R B 2019 *J. Cosmol. Astropart. Phys.* **08** 030
[16] Chen S B, Wang M Z and Jing J L 2020 *J. High Energy Phys.* **07** 054
[17] Zeng X X, Zhang H Q and Zhang H B 2020 *Eur. Phys. J. C* **80** 872
[18] Zeng X X and Zhang H Q 2020 *Eur. Phys. J. C* **80** 1058
[19] Peng J, Guo M Y and Feng X H 2021 *Phys. Rev. D* **104** 124010
[20] Li G P and He K J 2021 *J. Cosmol. Astropart. Phys.* **06** 037
[21] Zhou X, Chen S B and Jing J L 2022 *Sci. China Phys. Mech. Astron.* **65** 250411
[22] Zeng X X, He K J and Li G P 2022 *Sci. China Phys. Mech. Astron.* **65** 290411
[23] Li G P and He K J 2021 *Eur. Phys. J. C* **81** 1018
[24] Gan Q Y, Wang P, Wu H W and Yang H T 2021 *Phys. Rev. D* **104** 024003
[25] Gan Q Y, Wang P, Wu H W and Yang H T 2021 *Phys. Rev. D* **104** 044049
[26] Hou Y H, Liu P, Guo M Y, Yan H P and Chen B 2022 *Class. Quant. Grav.* **39** 194001
[27] Guo W D, Wei S W and Liu Y X 2022 arXiv: 2203.13477 [gr-qc]
[28] Wang H M, Lin Z C and Wei S W 2022 *Nucl. Phys. B* **985** 116026
[29] Hou Y H, Zhang Z Y, Yan H P, Guo M Y and Chen B 2022 *Phys. Rev. D* **106** 064058
[30] Qin X, Chen S B, Zhang Z L and Jing J L 2022 *Astrophys. J.* **938** 2
[31] Chen Y Q, Guo G Z, Wang P, Wu H W and Yang H T 2022 *Sci. China Phys. Mech. Astron.* **65** 120412
[32] Hawking S W 1975 *Commun. Math. Phys.* **43** 199
[33] Kubizňók D and Mann R B 2012 *J. High Energy Phys.* **07** 033
[34] Cai R G, Cao L M, Li L and Yang R Q 2013 *J. High Energy Phys.* **9** 1
[35] He K J, Hu X Y and Zeng X X 2019 *Chin. Phys. C* **43** 125101
[36] Ökcü Ö and Aydıner E 2017 *Eur. Phys. J. C* **77** 24
[37] Guo S, Han Y and Li G P 2020 *Class. Quant. Grav.* **37** 085016
[38] Guo S, Huang Y L, He K J and Li G P 2021 *Mod. Phys. Lett. A* **36** 2150108
[39] Wei S W, Wang Y Q, Liu Y X and Mann R B N 2021 *Sci. China Phys. Mech. Astron.* **64** 270411
[40] Zhang M and Guo M Y 2020 *Eur. Phys. J. C* **80** 790
[41] Belhaj A, Chakhchi L, E1 Moumni H, Khalloufi J and Masmar K 2020 *Int. J. Mod. Phys. A* **35** 2050170
[42] Chamblin A, Emparan R, Johnson C V and Myers R C 1999 *Phys. Rev. D* **60** 064018
[43] Gunasekaran S, Kubiznak D and Mann R B 2012 *J. High Energy Phys.* **11** 110
[44] Belhaj A, Chabab M, E1 Moumni H and Sedra M B 2012 *Chin. Phys. Lett.* **29** 100401
[45] Hendi S H and Vahidinia M H 2013 *Phys. Rev. D* **88** 084045
[46] Liu Y Q, Zou D C and Wang B 2014 *J. High Energy Phys.* **09** 179
[47] Wei S W and Liu Y X 2015 *Phys. Rev. Lett.* **115** 111302
[48] Zhang J L, Cai R G and Yu H W 2015 *Phys. Rev. D* **91** 044028
[49] Belhaj A, Chabab M, Moumni H E1, Masmar K, Sedra M B and Segui A 2015 *J. High Energy Phys.* **05** 149
[50] Chabab M, E1 Moumni H and Masmar K 2016 *Eur. Phys. J. C* **76** 304
[51] Chabab M, E1 Moumni H, Iraoui S and Masmar K 2016 *Eur. Phys. J. C* **76** 676
[52] Zou D C, Liu Y Q and Yue R H 2017 *Eur. Phys. J. C* **77** 365
[53] Wei S W and Liu Y X 2018 *Phys. Rev. D* **97** 104027
[54] Chabab M, E1 Moumni H, Iraoui S, Masmar K and Zhizeh S 2018 *Phys. Lett. B* **781** 316
[55] Perlick V, Tsupko O Y and Bisnovatyi-Kogan G S 2018 *Phys. Rev. D* **97** 104062
[56] Zhang M, Yue R H and Yang Z Y 2015 *Chin. Phys. Lett.* **32** 20401
[57] Ma M S and Zhao R 2015 *Chin. Phys. Lett.* **32** 30401
[58] Singh T I 2015 *Chin. Phys. B* **24** 070401
[59] Ye B B, Chen J H and Wang Y J 2017 *Chin. Phys. B* **26** 090202
[60] Hu X Y, He K J, Li Z H and Li G P 2020 *Chin. Phys. B* **29** 050401
[61] Guo S, Li G R and Li G P 2022 *Chin. Phys. C* **46** 095101
[62] Novello M, De Lorenci V A, Salim J M and Klippert R 2000 *Phys. Rev. D* **61** 045001
[63] Allahyari A, Khodadi M, Vagnozzi S and Mota D F 2020 *J. Cosmol. Astropart. Phys.* **02** 003
[64] Zeng X X, He K J, Li G P, Liang E W and Guo S 2022 *Eur. Phys. J. C* **82** 764
[65] Yu S and Gao C J 2020 *Int. J. Mod. Phys. D* **29** 2050032
[66] De Lorenci V A, Klippert R, Novello M and Salim J M 2000 *Phys. Lett. B* **482** 134
[67] Kruglov S I 2020 *Mod. Phys. Lett. A* **35** 2050291
[68] Cai X C and Miao Y G 2021 arXiv:2107.08352 [gr-qc]
[69] Wang C, Wu B, Xu Z M and Yang W L 2022 *Nucl. Phys. B* **976** 115698
[70] Eiroa E F and Sendra C M 2018 *Eur. Phys. J. C* **78** 91